TRITA-EPP-91-03

A NUMERICAL MODEL OF IONOSPHERIC CONVECTION DERIVED FROM FIELD-ALIGNED CURRENTS AND THE CORRESPONDING CONDUCTIVITY

L. G. Blomberg and G. T. Marklund

Report TRITA-EPP-91-03*

Department of Plasma Physics
Alfvén Laboratory
Royal Institute of Technology
S-100 44 Stockholm, Sweden

August 1991

* Supersedes TRITA-EPP-88-03

Abstract. A numerical model for the calculation of ionospheric convection patterns from given distributions of field-aligned current and ionospheric conductivity is described. The model includes a coupling between the conductivity and the field-aligned current, so that the conductivity peaks in regions of upward current, as is usually observed by measurements. The model is very flexible in that the input distributions, the field-aligned current and the conductivity, have been parametrized in a convenient way. From the primary model output, namely the ionospheric electrostatic potential (or convection) in the corotating frame, a number of other quantities can be computed. These include: the potential in the inertial frame (the transformation takes into account the non-alignment of the Earth's magnetic and geographic axes), the potential in the magnetospheric equatorial plane (projected using either a dipole magnetic field model or the Tsyganenko-Usmanov model, and the assumption of either vanishing parallel electric field or a proportionality between parallel potential and upward field-aligned current), the distribution of ionospheric (horizontal) current, and the Joule heating in the ionosphere. This model has been used together with a new snapshot technique to calculate the high-latitude potential distribution prevailing during a particular event by combining information from global auroral images and local measurements of fields and particles. The model potential variation along the satellite orbit was found to be in excellent agreement with that calculated from the measured electric field. The model has also been used to study some fundamental properties of the electrodynamics of the high-latitude ionosphere. The results of these different applications of the model have been published separately.

Contents

1. Introduction

The magnetosphere-ionosphere system, which is set up and powered by the interaction of the solar wind with the Earth's magnetic field, is a system which is characterized by a strong electrodynamical coupling. Electrical power is extracted by the magnetosphere from the solar wind in MHD type generators at the dayside magnetopause, in the magnetospheric boundary layers, and in the distant magnetotail, as the solar wind streams past or penetrates these regions. From the magnetospheric perspective the conducting ionosphere generally acts as a load, but it may in regions of auroral activity at times also act as a secondary generator, feeding electrical energy back into the magnetosphere. Generally though, the ionosphere as a whole is dissipative, and thus there is a net flow of electrical energy from the magnetosphere to the ionosphere.

Realistic models of the relationship between field-aligned currents, the ionospheric electric field, and the ionospheric conductivity are necessary for the understanding of the large-scale behaviour of this complex system. In this kind of models, one of the quantities is calculated given the other two. Over the past decade or so, numerous such models, employing different kinds of average input distributions have been developed [e.g., *Nisbet et al.*, 1978; *Kamide and Matsushita*, 1979*a*, *b*; *Gizler et al.*, 1979; *Bleuler et al.*, 1982]. Recently, models using input data inferred from and calibrated against satellite and/or ground-based data, have been developed. Among those is the method of calculating the instantaneous high-latitude potential distribution by *Marklund et al.* [1987*a*, *b*; 1988, 1991; *Marklund and Blomberg*, 1991*b*] which utilizes satellite imager and in situ data to obtain global input distributions of the field-aligned current and the ionospheric conductivity. Another, similar, approach is used in the work by *Kamide et al.* [1986] who use a conductivity distribution inferred from auroral images and an ionospheric current inferred from ground magnetometer data to calculate the convection. This technique has been further developed by *Richmond and Kamide* [1988].

The purpose of the present paper is to describe in detail the model used by *Marklund et al.* [1987*a*, *b*; 1988; 1991], *Blomberg and Marklund* [1988; 1991], and *Marklund and Blomberg* [1991*a*, *b*].

2. The model

The calculation of the electrostatic potential distribution has been performed using spherical (surface) coordinates, where the θ-coordinate is magnetic colatitude and the ϕ-coordinate corresponds to magnetic local time (MLT). The numerical solution is based on a finite difference scheme and the Successive Over-Relaxation (SOR) method. The boundary condition most commonly used in our applications is that the magnetic equator is an equipotential curve. The basic equations, the parametrization of the input quantities, the possible boundary conditions, the

primary and the various secondary output quantities, and the numerical solution are described in detail below.

2.1. Basic equations

The basic equation relating the height-integrated ionospheric (horizontal) current ($\mathbf{J}$) to the ionospheric electric field ($\mathbf{E}$) can be written

$$\mathbf{J} = \boldsymbol{\Sigma} \cdot (\mathbf{E} + \mathbf{v}_n \times \mathbf{B}) \tag{1}$$

where $\mathbf{E} + \mathbf{v}_n \times \mathbf{B}$ is the electric field in the "frame" of the neutral wind. $\mathbf{B}$ is the geomagnetic field, and $\boldsymbol{\Sigma}$ the height-integrated conductivity tensor. (The reason for using the frame of the neutral wind as the reference frame for defining the conductivity is that in this frame the horizontal conductivity tensor depends only on the usual Pedersen and Hall conductivies and the magnetic field inclination. In other frames additional anisotropizing effects enter since in these frames there is a preferred direction due to the bulk motion of neutral particles.) Our reference frame for the calculation is the Earth-fixed frame. In our applications of the model, we have hitherto assumed the neutral gas to corotate perfectly with the Earth, or in other words we have neglected upper atmospheric winds. Hence, in this case the frame of the neutral wind is equivalent to the Earth-fixed frame (i.e., $\mathbf{J} = \boldsymbol{\Sigma} \cdot \mathbf{E}$). (A quantitative investigation of the effects of different assumptions regarding the neutral wind distribution will be the subject of a future study.)

$\boldsymbol{\Sigma}$ is the height-integrated horizontal conductivity tensor (cf. Appendix A)

$$\boldsymbol{\Sigma} = \begin{bmatrix} \Sigma_{\theta\theta} & \Sigma_{\theta\phi} \\ \Sigma_{\phi\theta} & \Sigma_{\phi\phi} \end{bmatrix} \tag{2}$$

whose components (except at equatorial latitudes) are given by [e.g., *Rishbeth and Garriot*, 1969]

$$\Sigma_{\theta\theta} = \Sigma_P / \sin^2 I \tag{3a}$$

$$\Sigma_{\theta\phi} = -\Sigma_{\phi\theta} = \Sigma_H / \sin I \tag{3b}$$

$$\Sigma_{\phi\phi} = \Sigma_P \tag{3c}$$

where I is the inclination of the geomagnetic field ($\mathbf{B}$, which has been approximated by a dipole), and Σ_P and Σ_H are the height-integrated Pedersen and Hall conductivities, respectively.

The horizontal and field-aligned (positive downwards) components of the current are related through

$$\nabla \cdot \mathbf{J} = j_{\parallel} \cdot \sin I \tag{4}$$

Since in the Earth-fixed frame the geomagnetic field does not vary with time, Faraday's law (which is valid in inertial as well as non-inertial frames of reference)

tells us that we can represent the electric field by an electrostatic potential, Φ, (so that $\mathbf{E} = -\nabla\Phi$). Using Φ (4) can be written:

$$\nabla \cdot (\boldsymbol{\Sigma} \nabla \Phi) = -j_{\parallel} \cdot \sin I \tag{5}$$

This elliptic equation is the central equation in the present model.

A more detailed discussion of the conductivities and of height-integrated quantities is found in Appendix A.

2.2. Input quantities

The input quantities to the model are the field-aligned current and the ionospheric conductivity. In addition to this a boundary condition for the potential has to be given.

The primary mediator of the strong electrodynamical interaction between the magnetosphere and the ionosphere is field-aligned currents, currents flowing along the magnetic field lines linking the ionosphere to the magnetosphere. It is often argued that electric fields "map" along magnetic field lines, or in other words that the magnetic field lines are equipotential. Due to this mapping it is assumed that magnetospheric electric fields are "transmitted" along the magnetic field lines to the ionosphere. In this picture field-aligned currents play a secondary role. It should however be remembered that a fundamental requirement for a perfect electrical coupling along field lines is that the plasma has an infinite current-carrying ability. This is not always a valid approximation. For this reason, we regard the field-aligned current as the most fundamental quantity for describing the electrodynamical interaction between the ionosphere and the magnetosphere, irrespective of whether the magnetospheric generators most closely resemble current or voltage generators.

Some studies of satellite data indicate that the generators in the magnetosphere during quiet conditions on a large spatial scale behave as a voltage source in Region 1 and as a combination of voltage and current sources in Region 2 [e.g., *Fujii and Iijima*, 1987]. Others have found that the magnetospheric generators on the intermediate spatial scale in both regions behave essentially as a constant current source [e.g., *Vickrey et al.*, 1986].

Regardless of the extent to which the real magnetospheric generators act as voltage and/or current generators, there are several practical reasons (in addition to the physical reasons discussed above) for choosing the conductivity and the field-aligned current as input in the present model (i.e., assuming a current-driven system). As the large-scale field-aligned currents are generally confined to a relatively limited region of the ionosphere (where large-scale auroral features are seen), it is possible to describe the distribution of the field-aligned current with a reasonable number of parameters. Also, one of the most important ingredients in the method of *Marklund et al.* [1987*a*, *b*; 1988] is the use of satellite auroral

imager data. These are used to determine the "auroral geography," or in other words, to infer qualitatively the distribution of field-aligned currents and conductivity enhancement. Furthermore, by using the field-aligned current as input data, the conductivity which is partly coupled to the field-aligned current, becomes fully defined without the need for some recursive process.

The present numerical model has been refined and "tuned" to new applications in a number a steps. In the first version of the model it was only possible to specify field-aligned currents in region 1, region 2, and the cusp area. In later versions it is possible to specify an arbitrary field-aligned current distribution. We have also introduced a possibility to represent large-scale NBZ type currents and currents associated with transpolar arcs in an idealized way using a small number of additional coefficients.

It should be noted that although at first glance it seems obvious that the possibility to specify an arbitrary spatial distribution of the input quantities is a definite advantage, it is usually more practical for theoretical investigations to be able to describe the input quantities with a minimum of parameters. Thus, the more general way of specifying the field-aligned current supplements rather than replaces the older way. The different parametrizations of the input quantities are described below.

2.2.1. The field-aligned current

In the basic version of the model the ordinary Region 1 and Region 2 field-aligned currents [cf. *Iijima and Potemra*, 1976*a*; 1978], as well as the cusp currents [*Iijima and Potemra*, 1976*b*] can be represented. The basic parameters defining the geometry of the current systems are:

θ_{00} : colatitude of the dayside Region 1/2 interface
$\Delta\theta_0$: difference between nightside and dayside interface locations
$\Delta\theta_1$: the latitudinal width of Region 1
$\Delta\theta_2$: the latitudinal width of Region 2
$\Delta\theta_C$: the latitudinal width of the cusp

The centre of the auroral oval (assumed to coincide with the Region 1/2 interface) is described in this study by

$$\theta_0 = \theta_{00} + \Delta\theta_0 \cdot \left|\cos\frac{\phi}{2}\right| \tag{6}$$

The meaning of these geometrical parameters is illustrated in Figure 1. The longitudinal amplitude distribution of the Region 1 and Region 2 currents are specified by separate Fourier series (the number of terms included in the series is a free parameter). These series define the currents at the colatitudes $\theta_0 - \frac{\Delta\theta_1+\Delta\theta_2}{6}$ and $\theta_0 + \frac{\Delta\theta_1+\Delta\theta_2}{6}$, respectively. For each longitude, a third-order polynomial is computed which assumes the values of the Fourier series at the two colatitudes and

which vanishes at the poleward edge of Region 1 and at the equatorward edge of Region 2. In this way a continuous two-dimensional distribution of the current is obtained. In a similar way the cusp current is defined by a Fourier series representing the amplitude of the current at the centre of the cusp region together with a second-order polynomial describing the latitudinal variation.

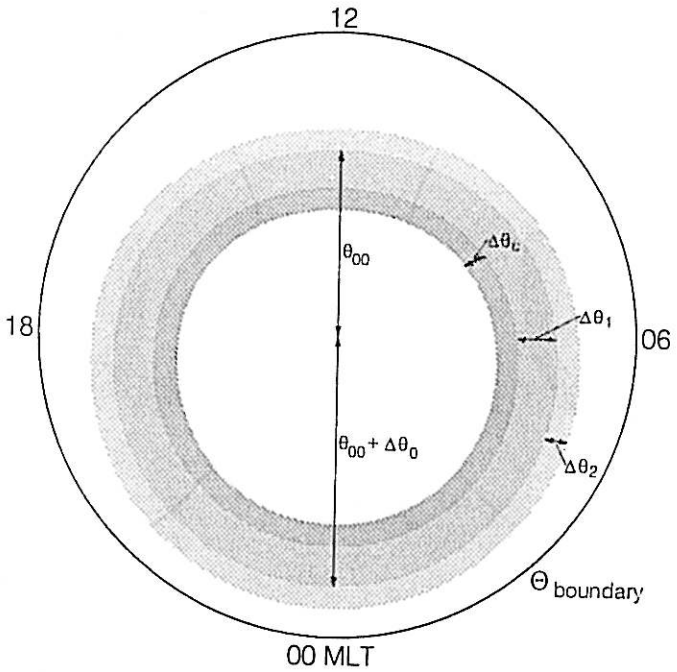

Fig. 1. Parameters describing the geometry of the current system. For further explanation see text.

"Polar-cap" field-aligned currents are represented (in later versions of the model) by a number of Sun-aligned (i.e., aligned in the local noon-midnight direction) current sheets (Figure 2). The amplitude variation with x within each sheet is given by a polynomial (of variable degree), while the y-variation is parabolic. Since the width (Δy) of each sheet is variable, wide NBZ type current systems as well as narrow transpolar-arc associated currents can be represented in this way.

Finally, there is a possibility to assign a specific value to the field-aligned current at each mesh point. This can be done in many different ways. One possibility that has been exploited in connection with event modelling (see overview of applications below) is to use an auroral image from the Viking spacecraft to infer not only the location but also the relative intensity of upward field-aligned currents. This can be done with reasonable accuracy since field-aligned currents are known to be carried predominantly by electrons, and thus upward currents correspond to precipitating electrons. There is no corresponding way of inferring the downward currents from the auroral emissions. The distribution of downward currents has to be based on general knowledge of statistical current patterns and how the current generally closes in the ionosphere, supplemented with calibration to magnetometer

measurements along a few satellite tracks. This means that the downward current is a much more uncertain parameter than the upward current. As part of our modelling effort we have developed a simple "graphical editor" for defining the field-aligned currents starting from a digitized auroral image.

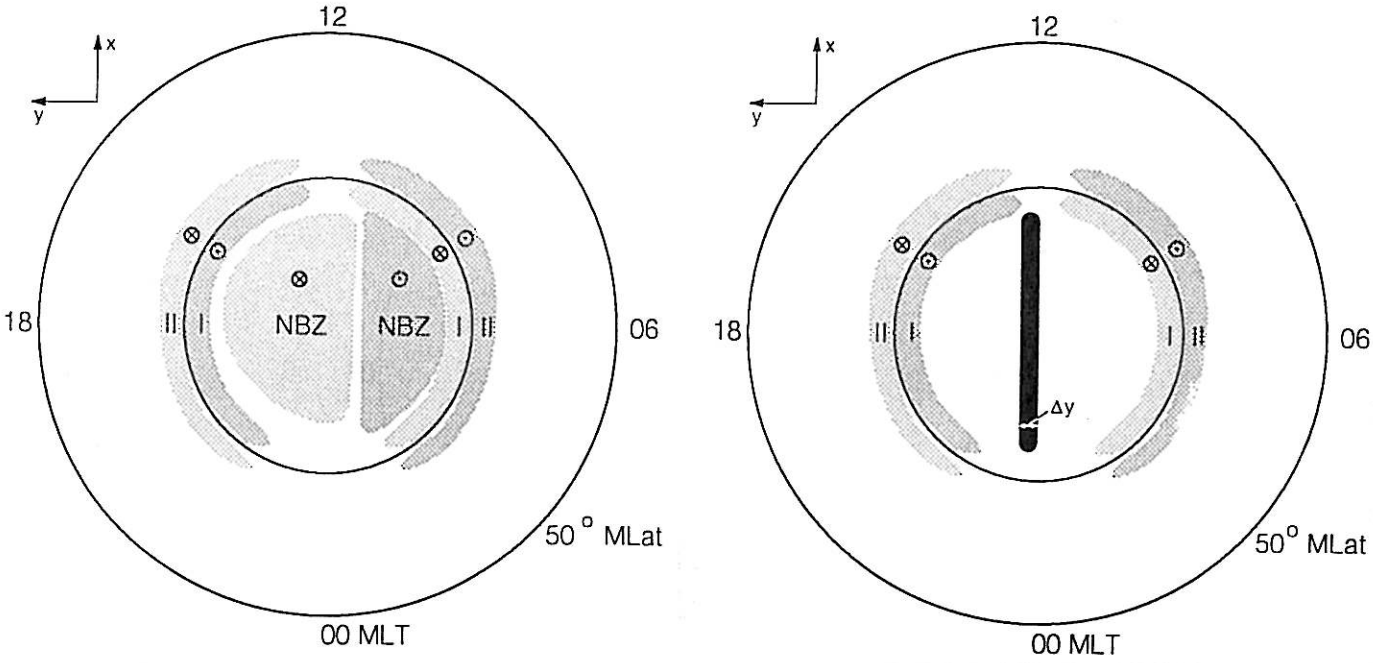

Fig. 2. Examples of field-aligned current geometries including "polar-cap" currents. To the left is a situation with extended NBZ-type currents in the "polar cap" representative of negative IMF B_y in the northern hemisphere. To the right is a situation with a single sheet of upward current, presumably related to a bright polar arc, in the "polar cap."

2.2.2. The ionospheric conductivity

The height-integrated conductivities are represented by

$$\Sigma_P = \sqrt{\Sigma_{0P}^2 + \Sigma_{gP}^2 + \Sigma_{UVP}^2 + \Sigma_{j_\parallel P}^2} \qquad (7a)$$

$$\Sigma_H = \sqrt{\Sigma_{0H}^2 + \Sigma_{gH}^2 + \Sigma_{UVH}^2 + \Sigma_{j_\parallel H}^2} \qquad (7b)$$

The root-sum-square relation is employed since the various ionization processes giving rise to the conductivity take place roughly within the same altitude range, and hence, as discussed by, for example, *Wallis and Budzinski* [1981], addition of the ionization rates (proportional to n_e^2, if balanced by recombination) gives a far more accurate estimate of the total conductivity (proportional to n_e) than a direct summation of the different conductivity contributions.

Σ_0 is a background term having a constant low value, representing the contribution from cosmic radiation and galactic EUV.

Σ_g represents an average auroral zone background conductivity given by

$$\Sigma_g = \Sigma_{g0} \cdot \exp\left(-\frac{(\theta - \theta_0)^2}{\theta_{g0}^2}\right) \qquad (8)$$

Σ_{UV} represents the part of the conductivities related to ionization produced by solar EUV-radiation. It is given here by

$$\Sigma_{UV} = \alpha \cdot \sqrt{\cos \chi} \tag{9}$$

where χ is the solar zenith angle.

$\Sigma_{j_\parallel}$ represents the conductivity enhancement arising from electron precipitation associated with upward field-aligned currents and is described in detail in the next section.

2.2.3. Current-conductivity coupling

In the present model a relationship between the field-aligned current and the conductivity has been used, so that the conductivity peaks in regions of upward current. The form of this relation is:

$$\Sigma_{j_\parallel} = \begin{cases} k(\phi) \cdot |j_\parallel|, & \text{for } j_\parallel \text{ upward} \\ 0, & \text{for } j_\parallel \text{ downward} \end{cases} \tag{10}$$

The factor of proportionality $k(\phi)$ is local-time dependent to account for the differences in the hardness of the particle spectrum. Thus, it may be chosen to have a lower value on the dayside where the precipitation generally is softer than on the nightside. The contribution from protons to the total precipitated particle energy is estimated to be at most 10 to 20 per cent [*Hultqvist*, 1973] and is assumed here to be accounted for by Σ_g. Upflowing particles usually deplete rather than enhance the ionospheric ionization, since, typically, they have thermal energies. However, this effect does not significantly modify the height-integrated conductivity since the depletion occurs mainly above the E layer [cf. *Block and Fälthammar*, 1968]. The linear relationship between conductivity and current is justified by, for example, the rocket observations of *Lyons et al.* [1979] and the model work by *Fridman and Lemaire* [1980] together with the fact that the conductivity is roughly proportional to the square-root of the downward electron energy flux [cf. *Harel et al.*, 1981]. This and other aspects of the current-conductivity coupling are discussed in some detail by *Blomberg and Marklund* [1988]. Note that when applying the model to specific events the exact value of $k(\phi)$ can be calibrated to the values derived from local measurements of particles, magnetic fields, and electric fields. More generally it has to be adapted to the prevailing magnetic activity level, since the characteristic energy of the precipitating electrons is typically different for different levels of activity.

2.2.4. Current-parallel potential coupling

Due to their greater mobility electrons are the primary carriers of field-aligned currents. For global current closure they must be able to flow both upward and downward along the magnetic field lines. The parallel motion of downward going electrons will be inhibited by the magnetic mirror force. To enable a sufficient

current to flow, parallel potential drops (widening the loss cones) are set up between the ionosphere and the magnetosphere. These potential drops are usually found to depend linearly on the upward field-aligned current. This coupling between the upward field-aligned current and the parallel (magnetic-field aligned) potential drop between the magnetosphere (magnetospheric generator) and the ionosphere (ionospheric load) is another coupling of importance to the modelling. This does not influence the input quantities but is of significance when projecting the calculated ionospheric potential distribution to the magnetospheric equatorial plane (or to an altitude above the acceleration region, for comparison with the electric field measured on high-altitude spacecraft). Theoretical studies [*Knight*, 1973; *Fälthammar*, 1978; *Fridman and Lemaire*, 1980] suggest a linear relationship between current and potential for potential drops in the range from a few hundred volts to several tens of kilovolts for realistic values of source region densities and temperatures. The assumptions made are: that the potential distribution varies monotonically along the field line; that the ionospheric and the magnetospheric plasmas can be represented by bi-Maxwellian distributions; and that sufficient pitch angle scattering is present in the source regions to maintain the loss cones. These assumptions are likely to be satisfied in general on auroral field lines. Observational evidence for this linear dependence has been documented by *Lyons et al.* [1979]. *Fälthammar* [1978] calculated a value of $\frac{dj_\parallel}{dV_\parallel}$ of $3\mu\mathrm{Am}^{-2}/\mathrm{kV}$ for source parameters typical of the plasma sheet. However, the linear relationship between current and potential drop sometimes breaks down and a saturation current flows. Such a situation is discussed by, for example, *Brüning et al.* [1990].

A projection of the calculated potential pattern for a specific event using a current-dependent parallel potential has been discussed by *Marklund et al.* [1991*b*].

2.2.5. Boundary conditions

The boundary is in the present model always a circle of constant latitude. Along this boundary two different types of boundary conditions are possible. One where the potential is specified as a function of azimuthal angle (Dirichlet condition) and one where the normal derivative of the potential (meridional electric field) is assumed zero along the boundary (homogeneous Neumann condition). For Neumann conditions the potential has to be fixed at one point on the boundary. Here we choose to set the potential to zero at $\phi = 0^\circ$ (0 hours MLT).

Generally speaking, the exact form of the boundary condition is more important the closer to the region of interest the boundary is located. If the magnetic equator is chosen as boundary and we are only interested in the potential distribution at auroral latitudes, the boundary condition is insignificant (within reasonable limits). In most of our applications of the model we have used a homogeneous

Dirichlet condition at the magnetic equator. For studies focussing on the penetration of auroral electric fields to lower latitudes the solution is more sensitive to the particular choice of boundary condition [cf. *Fontaine et al.*, 1985].

A way to overcome the possible problem of choosing a relevant boundary condition would be to extend the calculation to both hemispheres. In this case the region of interest will be "naturally closed" and it would only be necessary to fix the potential at one point, say, one of the poles. Such an extension is planned for a future date.

2.3. Model output

The output from the model, the electrostatic potential in the Earth-fixed frame, is obtained by solving Eq. 5 numerically. From this primary output quantity a number of other, secondary output quantities can be computed. The various output quantities will be described in detail below.

2.3.1. The potential in the corotating (Earth-fixed) frame

Strictly speaking, the output from the model represents the "Earth-fixed electric field" only if the neutral gas is at rest in this frame. This is, of course, never true in a strict sense. However, it is believed to be a reasonably good approximation, in most situations. Therefore, we take the primary output potential from the model to represent the potential in the corotating frame.

2.3.2. The "potential" in other frames

To obtain the electric field in an inertial frame of reference it is necessary to subtract the $\mathbf{v} \times \mathbf{B}$ electric field induced by Earth's rotation from the field in the corotating frame. For this purpose the geomagnetic field can, without introducing too much error, be represented by a centred dipole. If this dipole is assumed to be aligned with the geographic axis the transformation is done by simply adding the corotation potential:

$$\Phi_{\text{corot}} = -\frac{\mu_0 p \omega}{4\pi R_{\text{E}}} \sin^2 \theta \tag{11}$$

where p is the magnetic dipole moment, ω the angular velocity of Earth's rotation, R_{E} the radius of the Earth, and θ the colatitude.

If the dipole tilt is taken into account the situation becomes more complicated. In this case no inertial electrostatic potential exists since $\nabla \times \mathbf{E} = -\frac{\partial \mathbf{B}}{\partial t}$ does not vanish identically in any inertial frame of reference. Helmholtz-decomposing the $\mathbf{v} \times \mathbf{B}$ electric field we obtain one curl-free component which can be represented by a scalar potential, and one divergence-free component (representing a solenoidal "induced" electric field) which is more difficult to handle (in principle it can be represented by a vector potential but this is of limited use to us). The solenoidal component can be accounted for partly by introducing a "pseudo-potential" as discussed below. A detailed treatment of the corotation electric field is found in Appendix B.

If $\mathbf{v}$ describes rigid rotation (i.e., $\mathbf{v} = \boldsymbol{\omega} \times \mathbf{r}$) and the magnetic vector potential $\mathbf{A}$ (i.e., $\nabla \times \mathbf{A} = \mathbf{B}$), in the Coulomb gauge (i.e., $\nabla \cdot \mathbf{A} = 0$), is introduced then (cf. Appendix B)

$$\mathbf{v} \times \mathbf{B} = \nabla(\mathbf{v} \cdot \mathbf{A}) + \nabla \times (\mathbf{v} \times \mathbf{A}) \tag{12}$$

Hence, a potential function for the curl-free part of the corotation electric field can be defined:

$$\Phi_{\text{corot}'} = \mathbf{v} \cdot \mathbf{A} \tag{13}$$

Since for a dipole

$$\mathbf{A} = \frac{\mu_0}{4\pi} \frac{\mathbf{p} \times \mathbf{r}}{r^3} \tag{14}$$

this potential can be written:

$$\Phi_{\text{corot}'} = \frac{\mu_0 p \omega}{4\pi R_{\text{E}}} \left[\sin\theta_0 \cos(\phi_0 - \phi) \frac{\sin 2\theta}{2} - \cos\theta_0 \sin^2\theta \right] \tag{15}$$

where θ and ϕ are magnetic colatitude and magnetic local time, respectively, and subscript 0 refers to the north geographic pole. Note that ϕ_0 depends on the universal time.

If the solenoidal part of the corotation electric field is taken into account, the field is no longer curl-free, and does not possess a scalar potential. However, a "pseudo-potential" can be defined by the meridional integral of the electric field. Although such a "potential" does not represent the total electric field (i.e., $\mathbf{E} \neq -\nabla\Phi$), it does give a correct result for the meridional component (i.e., $E_\theta = -\frac{1}{r}\frac{\partial\Phi}{\partial\theta}$). Furthermore, as a consequence of this, the cross polar cap integral of the electric field in the inertial frame arising from corotation is correctly predicted. (Conventionally, the cross polar cap integral of the electric field is referred to as the "polar cap potential drop." In view of the present discussion, this is not appropriate in all frames.) Since this is an important parameter in theories and models, it makes sense to define this kind of "pseudo-potential." Thus, choosing the north magnetic pole as the zero-point and integrating the corotation electric field along magnetic meridians, the following expression results:

$$\text{“}\Phi\text{”}_{\text{corot}''} = \frac{\mu_0 p \omega}{4\pi R_{\text{E}}} \left[\sin\theta_0 \cos(\phi_0 - \phi) \left(\frac{\sin 2\theta}{2} + \theta \right) - \cos\theta_0 \sin^2\theta \right] \tag{16}$$

In this equation the last term represents the axially symmetrical part of the corotation potential, while the first part represents an asymmetric (UT dependent) contribution. Comparing the expressions for $\Phi_{\text{corot}'}$ and $\text{“}\Phi\text{”}_{\text{corot}''}$ we find that the potential and the solenoidal parts of the corotation electric field contribute almost equally to the asymmetry at polar latitudes.

All three above mentioned possibilities of representing the corotation "potential" are included in the model. Note that the choice of transformation is not trivial. Since the entire magnetosphere "wobbles" along with the rotating Earth,

the inertial frame might not be the optimal frame for describing the magnetospheric electric field. A more thorough study of corotation effects is planned for a future date.

2.3.3. The potential in the magnetosphere

The potential distribution in the ionosphere can be projected into the magnetosphere. This projection can be done either onto the equatorial plane or to the altitude of a given spacecraft for comparison with the measured electric field. The projection is done under the assumption of either perfect mapping (i.e., no magnetic-field aligned (parallel) electric fields), or that the parallel potential drop is proportional to the field-aligned current density in regions where the current is upward. The projection to spacecraft altitude depends on an assumption of how much of the total parallel potential drop that appears between the spacecraft and the ionosphere. For high-altitude (i.e., $> 1.5 - 2R_E$) spacecraft it is resonable to assume that the entire potential drop is located below the spacecraft. The projection to the equatorial plane depends on the magnetic field model employed. To date we have employed two different models of the magnetic field. The simplest one is a centred dipole. In this case the projection is given by:

$$r_{eq} = R_E \sin^{-2}\theta \qquad (17a)$$

$$\phi_{eq} = \phi \qquad (17b)$$

where r_{eq} and ϕ_{eq} are radial distance and azimuthal angle in the equatorial plane, respectively.

The other field model (or rather set of models) is the Tsyganenko-Usmanov model [*Tsyganenko and Usmanov*, 1982; *Tsyganenko*, 1987; 1989] combined with the IGRF (International Geomagnetic Reference Field) model [*IAGA Division I Working Group* 1, 1981; 1985]. This model takes into account not only the Earth's magnetic field (represented by IGRF), but also includes contributions from the ring current, the magnetotail currents, the magnetopause currents and the average effect of field-aligned currents. The latter model is furthermore K_p-dependent. For this case no simple relationship exists between colatitude and longitude in the ionosphere and the point where the field line intersects the equatorial plane, but the projection has to be done by numerical field line tracing.

2.3.4. Ionospheric currents

The ionospheric (horizontal) current distribution can be computed from the electric field and the height-integrated conductivity (Eq. 1). This provides a possibility to make comparisons with the ionospheric current vectors inferred from ground-based magnetometer data. However, since several assumptions (e.g., the Hall to Pedersen current ratio and the extent to which the Pedersen, Hall and field-aligned currents are seen on the ground) are necessary to determine the height-integrated ionospheric current from ground-based magnetic measurements, these can only give a rough picture of the ionospheric current systems.

2.3.5. Ionospheric Joule heating

From the electric field and the height-integrated conductivity it is also possible to calculate the ionospheric Joule heating or electrical power dissipation using:

$$P_{\text{Joule}} = \mathbf{E} \cdot \mathbf{J} = \mathbf{E} \cdot \boldsymbol{\Sigma} \cdot \mathbf{E} = \Sigma_{\theta\theta} \cdot E_\theta^2 + \Sigma_{\phi\phi} \cdot E_\phi^2 \tag{18}$$

2.4. The numerical solution of the fundamental differential equation

The basic equation (Eq. 5) has been solved numerically using the finite difference method known as the Successive Over-Relaxation (SOR) method (variously referred to as the Accelerated Liebmann Method). The iterative process for Laplace's equation in an equidistant rectangular mesh is described by:

$$u_{i,j}^{n+1} = u_{i,j}^n + \beta R_{i,j}^n = u_{i,j}^n + \frac{\beta}{4}(u_{i-1,j}^{n+1} + u_{i+1,j}^n + u_{i,j-1}^{n+1} + u_{i,j+1}^n - 4u_{i,j}^n) \tag{19}$$

where u is the unknown, subscripts i and j are mesh indices and the superscript denotes the iteration number. This illustrates the principle behind the method. For the more complicated equation of interest to us a number of coefficients (which are functions of latitude and longitude but not of the dependent variable) enter as well as a source term. The details can be found in Appendix C.

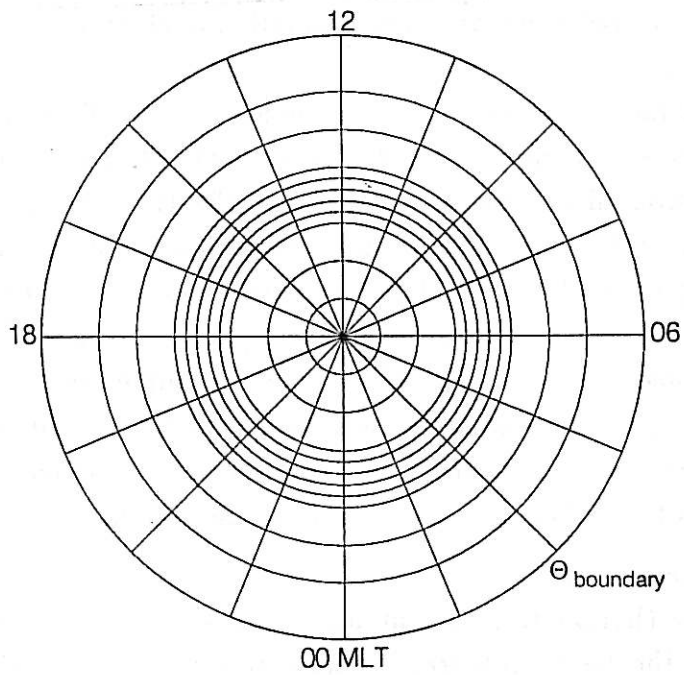

Fig. 3. Example of a mesh geometry typically used when studying situations without polar field-aligned current. The latitudinally dense part of the mesh coincides with the auroral zone where the region 1 and region 2 currents and the associated conductivity gradients are located. In situations where a polar current system is present the mesh is typically chosen to be dense also poleward of the oval.

The mesh used for the calculation is equidistant (in angular measures) in longitude but not in latitude. Due to the convergence of meridians towards the pole the mesh will be denser in longitude (measured in distances) at high latitudes. The possibility to use a variable latitudinal increment in the mesh makes it possible to obtain good spatial resolution in the "important" regions where significant variations in the potential are expected (e.g., the auroral zone), while keeping the number of mesh points at a reasonable level.

The over-relaxation factor, β, is either kept constant throughout the iterations or optimized using Carré's semi-empirical method. A new β_{opt} is then calculated every 25 iterations. The criterion used to determine numerical convergence is that the ratio of the norm of the last refinement vector (R) to the norm of the last solution vector should not exceed a specified value. The basic equations used for the finite difference discretization are summarized in Appendix C. General properties of the SOR method can be found in, for example, *Smith* [1965].

3. Brief review of some applications of the model

The model has to date been applied to a number of specific topics. It was first used by *Marklund et al.* [1987*a*, *b*; 1988]. They used simultaneous observations by the Viking and DMSP F7 spacecraft to obtain snapshot pictures of the high-latitude electrodynamics associated with a specific auroral situation viewed by the UV imager on Viking. The calculated potential pattern was in excellent agreement with that inferred from the electric field measured by Viking. The only significant discrepancies occured when the spacecraft was on field lines connected to acceleration regions, where deviations are to be expected due to the existence of parallel electric fields.

Another "snapshot study" was conducted by *Marklund et al.* [1991] using spacecraft data from Viking, DMSP F7, and Hilat. In this study the selected event was one where the interplanetary magnetic field (IMF) was northward and a transpolar arc was clearly seen in the Viking images. The resulting convection pattern was of the distorted two-cell type, with a sharp change of plasma flow direction at the location of the transpolar arc. The convection was, however, mostly antisunward in the polar region. Also in this study there was a good agreement between the calculated convection pattern and Viking electric field measurements.

It was also used by *Blomberg and Marklund* [1988] to study the influence on the high-latitude potential distribution of using a more realistic conductivity model including the field-aligned current-conductivity coupling. The main results were that the typical clockwise rotation of the polar cap electric field is reduced and that the electric field is significantly reduced in regions of upward current as compared to the results obtained using a local-time independent model of the particle-induced conductivity contribution.

Further, the model was used by *Blomberg and Marklund* [1991] to study high-latitude convection patterns "generated" by various large-scale (NBZ type) field-aligned current distributions, in particular currents representative of northward IMF. One of the main conclusions was that four-cell as well as three-cell large-scale convection patterns are compatible with the field-aligned current distributions that have been observed for northward IMF, and in particular that during a transition of the IMF from stably southward to stably northward (or vice versa) the convection pattern is likely to change from a two-cell type to a four-cell type (or vice versa), with a three-cell pattern showing up as an intermediate state.

In a related study [*Marklund and Blomberg*, 1991*a*], the model was used to examine convection patterns associated with smaller-scale field-aligned current systems (associated with transpolar arcs) at high latitudes. In particular it was shown that such transpolar-arc associated currents do not necessarily give rise to sunward convection in the "polar cap," nor is the large-scale convection pattern well described by a four-cell picture. Rather, the effect of such additional field-aligned currents is often quite local. However, in a real situation there might exist a combination of large-scale (NBZ type) currents and smaller-scale (transpolar-arc associated) currents, in which case the details of the convection system are more complicated. This will be discussed in a future paper (Blomberg and Marklund, manuscript in preparation, 1991).

Finally, the model has been used by *Marklund and Blomberg* [1991*b*] to illustrate how the magnetospheric convection pattern is modified when a parallel potential is introduced in regions of upward field-aligned current, "electrically decoupling" the magnetosphere from the ionosphere.

4. Summary

A flexible numerical model for calculating the ionospheric potential distribution given the distribution of field-aligned current and the corresponding (height-integrated) ionospheric conductivity has been developed. The model has been used both for theoretical investigations of the electrodynamics of the high-latitude ionosphere and for event studies using a newly developed "snapshot technique." An important feature in the model is a coupling between the conductivity and the upward field-aligned current, such that the conductivity peaks in regions of intense upward current. Such a relation between upward field-aligned current and ionospheric conductivity is usually observed by rockets and satellites. Apart from the primary output, the ionospheric potential distribution in the corotating frame of reference, there are several secondary output quantities. These include: the "potential" in the inertial frame, the potential projected to the magnetosphere, the ionospheric current vectors, and the ionospheric Joule heating. The projection to the magnetosphere can be done using different models of the magnetic field with the possibility to include a coupling between upward field-aligned current and the (parallel) potential drop between the ionosphere and the magnetosphere.

When projecting the potential to the magnetosphere the choice of frame in which to best describe the electric field is not trivial. The model provides three different possibilities to represent the transformation from the Earth-fixed to the inertial frame. Two of these transformations take into account the non-alignment of the Earth's magnetic and geographic axes, which makes the transformation universal-time dependent.

Even though the model in its present state is a useful tool for high-latitude ionospheric modelling, several extensions and refinements are possible. These include (but are not limited to): time dependence; explicit inclusion of neutral winds; a more quantitative coupling to the magnetosphere; and true global calculations (i.e., both hemispheres taken into account).

Appendix A

Conductivity in the collisional magnetized ionospheric plasma

The momentum equation for a charged particle (with charge q and mass m) in a magnetic field ($\mathbf{B}$) and a stationary background of neutrals reads:

$$m\frac{d\mathbf{v}}{dt} = q\mathbf{E} + q\mathbf{v}\times\mathbf{B} - \nu m\mathbf{v} \tag{A.1}$$

or, separating parallel and perpendicular (to $\mathbf{B}$) components

$$m\frac{dv_{\|}}{dt} = qE_{\|} - \nu m v_{\|} \tag{A.2a}$$

$$m\frac{d\mathbf{v}_{\perp}}{dt} = q\mathbf{E}_{\perp} + q\mathbf{v}_{\perp}\times\mathbf{B} - \nu m\mathbf{v}_{\perp} \tag{A.2b}$$

where $\mathbf{E}$ is the electric field and ν is the effective collision frequency (i.e., $-\nu m\mathbf{v}$ is the average momentum transfer rate). Taking $\mathbf{v}$ to mean the average velocity (over a time scale long compared to the collision time $1/\nu$, as well as to the gyration period $2\pi/\omega_c = 2\pi m/qB$) the left hand sides vanish. (We assume that collisions are frequent enough for a parallel conductivity to be meaningful). Beginning with the parallel component we obtain from (A.2a):

$$v_{\|} = \frac{q}{\nu m}E_{\|} \tag{A.3}$$

(the coefficient $q/\nu m$ is referred to as "mobility"). Vectorial multiplication of (A.2b) with $\mathbf{B}$ yields:

$$0 = q\mathbf{E}_{\perp}\times\mathbf{B} - q\mathbf{v}_{\perp}B^2 - \nu m\mathbf{v}_{\perp}\times\mathbf{B} \tag{A.4}$$

(A.2b) with a zero left-hand side and (A.4) give:

$$0 = q\mathbf{E}_{\perp} + \frac{q}{\nu m}\left(q\mathbf{E}_{\perp}\times\mathbf{B} - q\mathbf{v}_{\perp}B^2\right) - \nu m\mathbf{v}_{\perp} \tag{A.5}$$

Multiplying by ν/m and solving for $\mathbf{v}_{\perp}$ we obtain:

$$\mathbf{v}_{\perp} = \frac{1}{B}\frac{1}{{\omega_c}^2+\nu^2}\left(\frac{q}{|q|}\omega_c\nu\mathbf{E}_{\perp} - {\omega_c}^2\hat{\mathbf{B}}\times\mathbf{E}_{\perp}\right) \tag{A.6}$$

Thus, the electrical current driven by an electric field in the plasma is:

$$\begin{aligned}\mathbf{j} &= n_i q_i\mathbf{v}_i + n_e q_e\mathbf{v}_e = ne(\mathbf{v}_i - \mathbf{v}_e)\\ &= \frac{ne}{B}\left\{\left(\frac{\omega_{ce}\nu_e}{{\omega_{ce}}^2+{\nu_e}^2} + \frac{\omega_{ci}\nu_i}{{\omega_{ci}}^2+{\nu_i}^2}\right)\mathbf{E}_{\perp}\right.\\ &\quad\left. + \left(\frac{{\omega_{ce}}^2}{{\omega_{ce}}^2+{\nu_e}^2} - \frac{{\omega_{ci}}^2}{{\omega_{ci}}^2+{\nu_i}^2}\right)\hat{\mathbf{B}}\times\mathbf{E}_{\perp}\right\} + \frac{ne^2}{\nu m}\mathbf{E}_{\|}\\ &= \sigma_P\mathbf{E}_{\perp} + \sigma_H\hat{\mathbf{B}}\times\mathbf{E}_{\perp} + \sigma_{\|}\mathbf{E}_{\|}\end{aligned} \tag{A.7}$$

where we have introduced the direct ($\sigma_{\|}$), the Pedersen (σ_P), and the Hall (σ_H) conductivities. Subscripts e and i refer to electrons and ions, respectively.

In the ionosphere, the Pedersen current is primarily carried by ions, while the Hall current is primarily carried by electrons. The reason for this is the different ratios of collision to gyro frequency for ions and electrons. Expressed in the usual nomenclature for magnetized plasmas [e.g., *Alfvén and Fälthammar*, 1963], the ionospheric plasma is of high density from the point of view of the ions, but of medium density from the point of view of the electrons. In other words, the (perpendicular) motion of the ions is mostly controlled by collisions (with neutrals), while the (perpendicular) motion of the electrons is mostly controlled by the magnetic field.

Equation (A.7) applies in a frame where the neutrals are at rest. In a frame ($'$) where the neutral gas velocity is $\mathbf{v}_n$, the corresponding equation reads:

$$\mathbf{j} = \sigma_P(\mathbf{E}'_\perp + \mathbf{v}_n \times \mathbf{B}) + \sigma_H \hat{\mathbf{B}} \times (\mathbf{E}'_\perp + \mathbf{v}_n \times \mathbf{B}) + \sigma_\parallel \mathbf{E}'_\parallel \tag{A.8}$$

The ionosphere as a conducting layer

Following *Rishbeth and Garriot* [1969] we consider the ionosphere as a conducting layer. (This treatment was originally proposed by *Baker and Martyn* [1953].) In a local Cartesian coordinate system ($'$) where the z'-axis is anti-parallel to the magnetic field, the conductivity tensor is:

$$\sigma' = \begin{bmatrix} \sigma_P & \sigma_H & 0 \\ -\sigma_H & \sigma_P & 0 \\ 0 & 0 & \sigma_\parallel \end{bmatrix} \tag{A.9}$$

This is true irrespective of the orientation of the x' and y' axes. We choose here the x'-axis to be in the plane defined by the local magnetic field and the magnetic dipole axis (x' is, thus, approximately southward at high northern latitudes).

However, we are mainly interested in a relation between the electric field and the current in the horizontal plane. Therefore, we introduce a local coordinate system where the z-axis is vertical, and where the magnetic field lies in the $x - z$-plane (i.e., x is towards magnetic south, and y towards magnetic east). This system differs from the primed one by a rotation around the y'-axis (coinciding with the y-axis). The rotation matrix, R, is:

$$R = \begin{bmatrix} \sin I & 0 & \cos I \\ 0 & 1 & 0 \\ -\cos I & 0 & \sin I \end{bmatrix} \tag{A.10}$$

where I is the magnetic field inclination. In this system the conductivity tensor is $\sigma = R\sigma' R^{-1}$,

$$\sigma = \begin{bmatrix} \sigma_P \sin^2 I + \sigma_\parallel \cos^2 I & \sigma_H \sin I & (\sigma_\parallel - \sigma_P)\sin I \cos I \\ -\sigma_H \sin I & \sigma_P & \sigma_H \cos I \\ (\sigma_\parallel - \sigma_P)\sin I \cos I & -\sigma_H \cos I & \sigma_P \cos^2 I + \sigma_\parallel \sin^2 I \end{bmatrix} \tag{A.11}$$

The ionosphere is here considered as a layer with a limited vertical extent. Further, it is assumed that the conductivity outside the layer is so small that the current flowing across the boundary is negligible. This is, actually, a rather realistic assumption, since it is mainly the E region that is conducting. Because of this, polarization charges are set up on the "boundaries." These charges give rise to a vertical electric field, E_z. Using $j_z = 0$ we can express E_z in E_x and E_y.

$$E_z = \frac{1}{\sigma_P \cos^2 I + \sigma_\parallel \sin^2 I}\left\{(\sigma_P - \sigma_\parallel)\sin I \cos I \cdot E_x + \sigma_H \cos I \cdot E_y\right\} \tag{A.12}$$

Using this expression for E_z a relation between horizontal current and horizontal electric field is obtained:

$$\begin{bmatrix} j_x \\ j_y \end{bmatrix} = \begin{bmatrix} \sigma_{xx} & \sigma_{xy} \\ -\sigma_{xy} & \sigma_{yy} \end{bmatrix} \cdot \begin{bmatrix} E_x \\ E_y \end{bmatrix} \tag{A.13}$$

where

$$\sigma_{xx} = \frac{\sigma_\parallel \sigma_P}{\sigma_\parallel \sin^2 I + \sigma_P \cos^2 I} \tag{A.14a}$$

$$\sigma_{xy} = \frac{\sigma_\parallel \sigma_H \sin I}{\sigma_\parallel \sin^2 I + \sigma_P \cos^2 I} \tag{A.14b}$$

$$\sigma_{yy} = \frac{{\sigma_H}^2 \cos^2 I}{\sigma_\parallel \sin^2 I + \sigma_P \cos^2 I} + \sigma_P \tag{A.14c}$$

Generally, $\sigma_\parallel \gg \sigma_P, \sigma_\parallel \gg \sigma_H$ so that except at equatorial latitudes, $\sigma_\parallel \sin^2 I \gg \sigma_P \cos^2 I$ and thus the following approximations valid:

$$\sigma_{xx} \approx \frac{\sigma_P}{\sin^2 I} \tag{A.15a}$$

$$\sigma_{xy} \approx \frac{\sigma_H}{\sin I} \tag{A.15b}$$

$$\sigma_{yy} \approx \sigma_P \tag{A.15c}$$

Height-integration of the ionospheric layer

When dealing with the large-scale electrodynamics of the ionosphere it is convenient, and customary, to introduce height-integrated quantities. The height-integrated conductivities are given by $\Sigma_P = \int \sigma_P dz$ and $\Sigma_H = \int \sigma_H dz$, respectively. The lower and upper limits of integration are usually 70-90 km and 160-220 km, respectively. The height-integrated horizontal current, $\mathbf{J}$, is defined in an analogous way.

To introduce a field-aligned current into our equations, we go back for a moment to the non-integrated quantities, and form the divergence of the current, which in steady-state vanishes

$$\nabla \cdot \mathbf{j} = \frac{\partial j_x}{\partial x} + \frac{\partial j_y}{\partial y} + \frac{\partial j_z}{\partial z} = 0 \tag{A.16}$$

Integrating this equation along z we obtain:

$$\frac{\partial}{\partial x}\int j_x dz + \frac{\partial}{\partial y}\int j_y dz + j_z(z_{max}) - j_z(z_{min}) = 0 \qquad \text{(A.17)}$$

The vertical current flow at the lower boundary is negligible. Hence, $j_z(z_{min}) = 0$. As discussed above, in case we let the ionosphere decide it will set up polarization charges to make the current vanish at the upper boundary as well. However, if there is an externally imposed current across the boundary there is nothing the ionosphere can do, but to let it flow. Hence, in this case, $j_z(z_{max}) = -j_{||}\sin I$, where $j_{||}$ is the field-aligned current (which by convention is taken positive for current flowing into the ionosphere). Thus,

$$\nabla \cdot \mathbf{J} = j_{||}\sin I \qquad \text{(A.18)}$$

where

$$\mathbf{J} = \mathbf{\Sigma}(\mathbf{E} + \mathbf{v}_n \times \mathbf{B}) \qquad \text{(A.19)}$$

$\mathbf{J}$ and $\mathbf{\Sigma}$ are here height-integrated quantities while $\mathbf{E}$ is assumed not to vary with altitude within the layer. (Strictly speaking $\nabla_\perp \cdot \mathbf{J}_\perp$ would be a more correct notation. However, the notation of equation (A.18) is the one customary in ionospheric electrodynamics.)

If the magnetic field inclination, I, is 90° the validity of the above equations is obvious. For other values of I this is less obvious. However, calculations by *Nisbet et al.* [1978] showed that, because the vertical extent of the ionosphere is small compared to its horizontal extent and because the sources of the current system are at high latitudes, both $E_z = 0$ and $j_z = 0$ are good approximations within the E region. (The assumption $j_z = 0$ was originally introduced by *Baker and Martyn* [1953]. Note that strictly speaking $E_z = 0$ is in conflict with our previous assumption that polarization charges are set up giving the E_z necessary to make $j_z = 0$. However, in practice both approximations may be used simultaneously.)

Furthermore, one of the conclusions from the study by *Nisbet et al.* [1978] was that "the dc fields and currents in the ionosphere on the scales being studied here are essentially independent of the field line conductivity." (They were studying large-scale effects.)

The concept of an ionospheric layer has proven very useful in modelling of ionospheric electrodynamics. Several studies have yielded realistic results using this approximation. However, for a complete quantitative picture of the ionospheric electrodynamics in general, and the electrodynamical coupling of the ionosphere to the magnetosphere in particular, fully three-dimensional models are probably needed.

Appendix B

For the purpose of describing the corotation electric field the Earth's magnetic field can be approximated by a centred dipole. Its vector potential, $\mathbf{A}$, is

$$\mathbf{A} = \frac{\mu_0}{4\pi}\frac{\mathbf{p}\times\mathbf{r}}{r^3} \tag{B.1}$$

The magnetic field (or more correctly magnetic flux density) $\mathbf{B}$ is

$$\mathbf{B} = \nabla\times\mathbf{A} = \frac{\mu_0}{4\pi}\nabla\left(\frac{\mathbf{p}\cdot\mathbf{r}}{r^3}\right) \tag{B.2}$$

Since $\mathbf{v} = \boldsymbol{\omega}\times\mathbf{r}$ (rigid rotation) the corotation electric field can be written

$$\mathbf{E}_{\text{corot}} = -\mathbf{v}\times\mathbf{B} = -(\boldsymbol{\omega}\times\mathbf{r})\times\mathbf{B} = (\mathbf{r}\cdot\mathbf{B})\boldsymbol{\omega} - (\boldsymbol{\omega}\cdot\mathbf{B})\mathbf{r} \tag{B.3}$$

Another expression for the corotation field is obtained by adding the well-known vector relations

$$\nabla(\mathbf{v}\cdot\mathbf{A}) = \mathbf{v}\times(\nabla\times\mathbf{A}) + \mathbf{A}\times(\nabla\times\mathbf{v}) + (\mathbf{v}\cdot\nabla)\mathbf{A} + (\mathbf{A}\cdot\nabla)\mathbf{v} \tag{B.4}$$

$$\nabla\times(\mathbf{v}\times\mathbf{A}) = (\mathbf{A}\cdot\nabla)\mathbf{v} - (\mathbf{v}\cdot\nabla)\mathbf{A} + \mathbf{v}\nabla\cdot\mathbf{A} - \mathbf{A}\nabla\cdot\mathbf{v} \tag{B.5}$$

Noting the relations:

$$\nabla\cdot\mathbf{A} = 0 \quad \text{(Gauge condition)} \tag{B.6}$$

$$\nabla\cdot\mathbf{v} = 0 \tag{B.7}$$

$$(\mathbf{A}\cdot\nabla)\mathbf{v} = \boldsymbol{\omega}\times\mathbf{A} \tag{B.8}$$

$$\nabla\times\mathbf{v} = 2\boldsymbol{\omega} \tag{B.9}$$

the following useful identity results

$$\mathbf{v}\times\mathbf{B} = \nabla(\mathbf{v}\cdot\mathbf{A}) + \nabla\times(\mathbf{v}\times\mathbf{A}) \tag{B.10}$$

The first term on the right hand side is curl-free and the second divergence-free. In other words the first term represents the potential part of the field while the second one represents the induction field.

The corotation field with a non-tilted magnetic axis

If the magnetic axis and the rotational axis are coaxial the $\mathbf{v}\times\mathbf{B}$-field is curl-free in the inertial frame and thus an electrostatic "corotation" potential can be readily defined (with the pole as the reference point) by integrating the meridional component of the $\mathbf{v}\times\mathbf{B}$-field along any meridian. Expressed in a spherical coordinate system where the polar axis is parallel with the magnetic and rotational axes (positive in the direction of the north geographic pole) this component equals $v_\phi B_r$ where $v_\phi = \omega R_{\text{E}}\sin\theta$ and $B_r = -\frac{\mu_0 p\cos\theta}{2\pi R_{\text{E}}^3}$. Here p is the magnetic dipole moment

and ω the angular velocity of Earth's rotation, while θ and ϕ are colatitude and longitude, respectively. The corotation potential at colatitude θ is then given by:

$$\Phi_{\text{corot}}(\theta,\phi) = \int_{\theta}^{0} E_{\theta} R_{\text{E}} d\theta = -\frac{\mu_0 p \omega}{4\pi R_{\text{E}}} \sin^2\theta \tag{B.11}$$

The corotation field with a tilted magnetic axis

If the magnetic and rotational axes are non-coaxial considerable complication arises. The corotation field is, of course, still given by $-\mathbf{v}\times\mathbf{B}$ but due to the dipole tilt $\frac{\partial \mathbf{B}}{\partial t} = -\nabla\times\mathbf{E} \not\equiv 0$ in the inertial frame and thus the corotation field is not derivable entirely from an electrostatic potential. Introducing a Cartesian coordinate system with the z-axis along the north magnetic axis, $\mathbf{r}$ and $\boldsymbol{\omega}$ are expressed as:

$$\mathbf{r} = r(\sin\theta\cos\phi, \sin\theta\sin\phi, \cos\theta) \tag{B.12}$$

$$\boldsymbol{\omega} = \omega\hat{\mathbf{r}}_0 = \omega(\sin\theta_0\cos\phi_0, \sin\theta_0\sin\phi_0, \cos\theta_0) \tag{B.13}$$

where subscript 0 refers to the north geographic pole. The latitudinal component of $\mathbf{E}_{\text{corot}}$, $E_{\theta_{\text{corot}}}$ is given by

$$E_{\theta_{\text{corot}}} = \mathbf{E}_{\text{corot}}\cdot\hat{\boldsymbol{\theta}} = (\mathbf{r}\cdot\mathbf{B})(\boldsymbol{\omega}\cdot\hat{\boldsymbol{\theta}}) \tag{B.14}$$

$\mathbf{r}\cdot\mathbf{B}$ equals rB_r which, since $\mathbf{B}$ is approximated here by a dipole (with dipole moment $\mathbf{p} = -p\hat{\mathbf{z}}$), can be written

$$\mathbf{r}\cdot\mathbf{B} = -r\frac{\mu_0}{2\pi}\frac{\cos\theta}{r^3}p \tag{B.15}$$

and, since

$$\hat{\boldsymbol{\theta}} = (\cos\theta\cos\phi, \cos\theta\sin\phi, -\sin\theta) \tag{B.16}$$

the explicit form of $\boldsymbol{\omega}\cdot\hat{\boldsymbol{\theta}}$ is

$$\boldsymbol{\omega}\cdot\hat{\boldsymbol{\theta}} = \omega[\sin\theta_0\cos\theta\cos(\phi_0-\phi) - \cos\theta_0\sin\theta] \tag{B.17}$$

Hence, the latitudinal component of $\mathbf{E}$ is

$$E_{\theta_{\text{corot}}} = -\frac{\mu_0\omega p}{2\pi}\frac{\cos\theta}{r^2}[\sin\theta_0\cos\theta\cos(\phi_0-\phi) - \cos\theta_0\sin\theta] \tag{B.18}$$

Thus far the treatment is completely general. Since $\nabla\times\mathbf{E}_{\text{corot}} \not\equiv 0$ no electrostatic potential representing $\mathbf{E}_{\text{corot}}$ exists. However, integrating this electric field along magnetic meridians, a "pseudo-potential," "Φ"$_{\text{corot}}$", representing the latitudinal component of $\mathbf{E}_{\text{corot}}$ is obtained:

$$\text{“}\Phi\text{”}_{\text{corot}}(\theta,\phi) = \frac{\mu_0 p\omega}{4\pi R_{\text{E}}}\left[\sin\theta_0\cos(\phi_0-\phi)\left(\frac{\sin 2\theta}{2}+\theta\right) - \cos\theta_0\sin^2\theta\right] \tag{B.19}$$

If we are only interested in the potential part of the corotation electric field, we find from (B.10) that the potential is given by $\mathbf{v} \cdot \mathbf{A}$. The explicit form of this potential, $\Phi_{\mathrm{corot}'}$, is

$$\begin{aligned}\Phi_{\mathrm{corot}'} = \mathbf{v} \cdot \mathbf{A} &= \frac{\mu_0}{4\pi r^3}(\boldsymbol{\omega} \times \mathbf{r}) \cdot (\mathbf{p} \times \mathbf{r}) \\ &= \frac{\mu_0 p \omega}{4\pi R_{\mathrm{E}}} \left[\sin\theta_0 \cos(\phi_0 - \phi) \frac{\sin 2\theta}{2} - \cos\theta_0 \sin^2\theta \right] \end{aligned} \tag{B.20}$$

In this expression we recognize two terms from (B.19). The last term in both equations represents the symmetrical part of the corotation potential (if the magnetic dipole is non-tilted (i.e., $\theta_0 = 0$) this is the only non-vanishing term in both equations). The first term in both equations represents the potential part of the asymmetry introduced by the dipole tilt. The term present in (B.19) but lacking in (B.20) represents the solenoidal part of this asymmetry. We see that at high latitudes (i.e., $\theta \ll \pi/2$) the potential and solenoidal contributions to the asymmetry are almost equal (since $(\sin 2\theta)/2 = \theta + O(\theta^3)$).

Appendix C

General considerations on the numerical solution

In principle, all finite difference methods for numerical solution of linear differential equations amount to solving a system of linear equations. For practical reasons this is usually done by an iterative process rather than by direct Gaussian elimination. Consider the system of equations $Ax = b$ where x and b are vectors, and A is a matrix that can be written $A = D(L + I + U)$ where D is a diagonal matrix, I the identity matrix, and L and U are lower and upper triangular matrices, having zeroes in their main diagonals. From this follows: $x = -(L + U)x + D^{-1}b$. This formulation is the basis for the simplest iterative process, known as the Newton-Jacobi method: $x^{(n+1)} = -(L+U)x^{(n)} + D^{-1}b$. Superscripts in parentheses denote iteration number. Here $(L + U)$ is the iteration matrix. Generally speaking the speed of convergence depends on the spectral radius (ρ) of the iteration matrix (which must be less than unity for the iteration process to converge at all). With the Newton-Jacobi formulation, convergence is usually quite slow.

Another possibility is to rewrite the equation in the following way: $(L + I)x = -Ux + D^{-1}b$. This leads to the Gauss-Seidel method: $x^{(n+1)} = -(L + I)^{-1}Ux^{(n)} + (L + I)^{-1}D^{-1}b$. Here the speed of convergence depends on $\rho((L + I)^{-1}U)$. This scheme is in general faster than the Newton-Jacobi scheme.

Faster convergence can often be obtained by extending the Gauss-Seidel formulation. Consider the following iteration matrix: $(I + \beta L)^{-1}((1 - \beta)I - \beta U)$. This corresponds to the Gauss-Seidel method (which is obtained by setting $\beta = 1$) but in each iteration the "correction" is greater (β should be in the range $1 < \beta < 2$) than what is predicted by the Gauss-Seidel method. In this way convergence can be speeded up. This method is known as the Successive Over-Relaxation method, and β is called the over-relaxation factor. Theoretically, β should be chosen to minimize the spectral radius of the iteration matrix. For certain classes of matrices it is possible to find an analytical expression for the optimum β. Often, however, a suitable value has to be found empirically. (If β is chosen such that ρ exceeds unity the iteration sequence will diverge.)

Details of the numerical solution

The explicit form of the basic differential equation (Eq. 5) is (assuming r = constant = 1) :

$$
\begin{aligned}
-j_{\|} \cdot \sin I = -\nabla \cdot \mathbf{J} &= -\nabla \cdot \left\{ \begin{bmatrix} \Sigma_{\theta\theta} & \Sigma_{\theta\phi} \\ -\Sigma_{\theta\phi} & \Sigma_{\phi\phi} \end{bmatrix} \begin{bmatrix} E_\theta \\ E_\phi \end{bmatrix} \right\} \\
&= \nabla \cdot \left[(\Sigma_{\theta\theta} \frac{\partial \Phi}{\partial \theta} + \Sigma_{\theta\phi} \frac{1}{\sin\theta} \frac{\partial \Phi}{\partial \phi}) \hat{\theta} + (-\Sigma_{\theta\phi} \frac{\partial \Phi}{\partial \theta} + \Sigma_{\phi\phi} \frac{1}{\sin\theta} \frac{\partial \Phi}{\partial \phi}) \hat{\phi} \right] \\
&= \Sigma_{\theta\theta} \frac{\partial^2 \Phi}{\partial \theta^2} + \frac{1}{\sin^2\theta} \Sigma_{\phi\phi} \frac{\partial^2 \Phi}{\partial \phi^2} + \left(\cot\theta \Sigma_{\theta\theta} + \frac{\partial \Sigma_{\theta\theta}}{\partial \theta} - \frac{1}{\sin\theta} \frac{\partial \Sigma_{\theta\phi}}{\partial \phi} \right) \frac{\partial \Phi}{\partial \theta} \\
&+ \left(\frac{1}{\sin\theta} \frac{\partial \Sigma_{\theta\phi}}{\partial \theta} + \frac{1}{\sin^2\theta} \frac{\partial \Sigma_{\phi\phi}}{\partial \phi} \right) \frac{\partial \Phi}{\partial \phi} \qquad \text{(C.1)}
\end{aligned}
$$

Mesh points for the numerical solution are $\{\theta_i\}_{i=1}^{I}$ and $\{\phi_j\}_{j=1}^{J}$. By Taylor expansion a finite difference approximation of derivatives can be obtained. Consider a Taylor expansion of the function $f(x)$:

$$f(x + h_+) = f(x) + h_+ f'(x) + \frac{h_+^2}{2} f''(x) + O(h_+^3)$$

$$f(x - h_-) = f(x) - h_- f'(x) + \frac{h_-^2}{2} f''(x) + O(h_-^3)$$

Neglecting terms of degree three and higher the two equations can be used to isolate $f'(x)$ and $f''(x)$. Extending this principle to two dimensions and introducing the notation:

$$\Phi_{i,j} = \Phi(\theta_i, \phi_j) \qquad \text{(C.2)}$$

$$h_- = \theta_i - \theta_{i-1} \qquad \text{(C.3)}$$

$$h_+ = \theta_{i+1} - \theta_i \qquad \text{(C.4)}$$

$$k_- = \phi_j - \phi_{j-1} \qquad \text{(C.5)}$$

$$k_+ = \phi_{j+1} - \phi_j \qquad \text{(C.6)}$$

the finite difference approximations of the various derivatives of interest to us can be written

$$\frac{\partial^2 \Phi}{\partial \theta^2} \leftrightarrow 2 \frac{h_- \Phi_{i+1,j} + h_+ \Phi_{i-1,j} - (h_+ + h_-) \Phi_{i,j}}{h_+ h_- (h_+ + h_-)} \qquad \text{(C.7)}$$

$$\frac{\partial \Phi}{\partial \theta} \leftrightarrow \frac{h_-^2 \Phi_{i+1,j} - h_+^2 \Phi_{i-1,j} - (h_-^2 - h_+^2) \Phi_{i,j}}{h_+ h_- (h_+ + h_-)} \qquad \text{(C.8)}$$

$$\frac{\partial^2 \Phi}{\partial \phi^2} \leftrightarrow 2 \frac{k_- \Phi_{i,j+1} + k_+ \Phi_{i,j-1} - (k_+ + k_-) \Phi_{i,j}}{k_+ k_- (k_+ + k_-)} \qquad \text{(C.9)}$$

$$\frac{\partial \Phi}{\partial \phi} \leftrightarrow \frac{k_-^2 \Phi_{i,j+1} - k_+^2 \Phi_{i,j-1} - (k_-^2 - k_+^2) \Phi_{i,j}}{k_+ k_- (k_+ + k_-)} \qquad \text{(C.10)}$$

Using these relations the following equation, which forms the basis for the evaluation of the iteration matrix in the SOR method, is obtained

$$\begin{aligned}
&\Phi_{i,j} \cdot \left[\frac{A}{h_+ h_-} + \frac{B}{k_+ k_-} + \frac{h_- - h_+}{h_+ h_-} C + \frac{k_- - k_+}{k_+ k_-} D \right] \\
&\quad = \Phi_{i+1,j} \cdot \left[\frac{A}{h_+(h_+ + h_-)} + \frac{h_- C}{h_+(h_+ + h_-)} \right] \\
&\quad + \Phi_{i-1,j} \cdot \left[\frac{A}{h_-(h_+ + h_-)} - \frac{h_+ C}{h_-(h_+ + h_-)} \right] \\
&\quad + \Phi_{i,j+1} \cdot \left[\frac{B}{k_+(k_+ + k_-)} + \frac{k_- D}{k_+(k_+ + k_-)} \right] \\
&\quad + \Phi_{i,j-1} \cdot \left[\frac{B}{k_-(k_+ + k_-)} - \frac{k_+ D}{k_-(k_+ + k_-)} \right] + j_{\|i,j} \cdot \sin I
\end{aligned} \tag{C.11}$$

where

$$A = 2 \cdot \Sigma_{\theta\theta} \tag{C.12}$$

$$B = \frac{2}{\sin^2 \theta} \Sigma_{\phi\phi} \tag{C.13}$$

$$C = \cot \theta \cdot \Sigma_{\theta\theta} + \frac{\partial \Sigma_{\theta\theta}}{\partial \theta} - \frac{1}{\sin \theta} \frac{\partial \Sigma_{\theta\phi}}{\partial \phi} \tag{C.14}$$

$$D = \frac{1}{\sin \theta} \frac{\partial \Sigma_{\theta\phi}}{\partial \theta} + \frac{1}{\sin^2 \theta} \frac{\partial \Sigma_{\phi\phi}}{\partial \phi} \tag{C.15}$$

References

Alfvén, H., and C.-G. Fälthammar, Cosmical Electrodynamics, 2nd ed., *Oxford University Press*, 1963.

Baker, W. G., and D. F. Martyn, Electric currents in the ionosphere, I, Conductivity, *Phil. Trans. Roy. Soc. London, Ser. A*, 246, 281, 1953.

Bleuler, E., C. H. Li, and J. S. Nisbet, Relationships between the Birkeland currents, ionospheric currents, and electric fields, *J. Geophys. Res., 87*, 757, 1982.

Block, L. P., and C.-G. Fälthammar, Effects of field-aligned currents on the structure of the ionosphere, *J. Geophys. Res., 73*, 4807, 1968.

Blomberg, L. G., and G. T. Marklund, The influence of conductivities consistent with field-aligned currents on high-latitude convection patterns, *J. Geophys. Res., 93*, 14493, 1988.

Blomberg, L. G., and G. T. Marklund, High-latitude convection patterns for various large-scale field-aligned current configurations, *Geophys. Res. Lett., 18*, 717, 1991.

Brüning, K., L. P. Block, G. T. Marklund, L. Eliasson, R. Pottelette, J. S. Murphree, T. A. Potemra, and S. Perraut, Viking observations above a postnoon aurora, *J. Geophys. Res., 95*, 6039, 1990.

Fontaine, D., M. Blanc, L. Reinhart, and R. Glowinski, Numerical simulations of the magnetospheric convection including effects of electron precipitation, *J. Geophys. Res., 90*, 8343, 1985.

Fridman, M., and J. Lemaire, Relationship between auroral electrons fluxes and field aligned potential difference, *J. Geophys. Res., 85*, 664, 1980.

Fujii, R., and T. Iijima, Control of the ionospheric conductivities on large-scale Birkeland current intensities under geomagnetic quiet conditions, *J. Geophys. Res., 92*, 4505, 1987.

Fälthammar, C.-G., Problems related to macroscopic electric fields in the magnetosphere, *Astrophys. Space Sci., 55*, 179, 1978.

Gizler, V. A., V. S. Semenov, and O. A. Troshichev, Electric fields and currents in the ionosphere generated by field-aligned currents observed by Triad, *Planet. Space Sci., 27*, 223, 1979.

Harel, M., R. A. Wolf, P. H. Reiff, R. W. Spiro, W. J. Burke, F. J. Rich, and M. Smiddy, Quantitative simulation of a magnetospheric substorm, 1, model logic and overview, *J. Geophys. Res., 86*, 2217, 1981.

Hultqvist, B., Auroral particles, pp. 161 in *Cosmical Geophysics*, Eds. A. Egeland, Ø. Holter, and A. Omholt, Scandinavian University Books, 1973.

IAGA Division I Working Group 1, International Geomagnetic Reference Fields: DGRF 1965, DGRF 1970, DGRF 1975, and IGRF 1980, *Eos Trans AGU, 62*, 1169, 1981.

IAGA Division I Working Group 1, International Geomagnetic Reference Field Revision 1985, *J. Geomag. Geoelectr. 37*, 1157, 1985.

Iijima, T., and T. A. Potemra, The amplitude distribution of field-aligned currents at northern high latitudes observed by Triad, *J. Geophys. Res., 81*, 2165, 1976*a*.

Iijima, T., and T. A. Potemra, Field-aligned current in the dayside cusp observed by Triad, *J. Geophys. Res., 81*, 5971, 1976*b*.

Iijima, T., and T. A. Potemra, Large-scale characteristics of field-aligned currents associated with substorms, *J. Geophys. Res., 83*, 599, 1978.

Kamide, Y., and S. Matsushita, Simulation studies of ionospheric electric fields and currents in relation to field-aligned currents, 1, quiet periods, *J. Geophys. Res., 84*, 4083, 1979*a*.

Kamide, Y., and S. Matsushita, Simulation studies of ionospheric electric fields and currents in relation to field-aligned currents, 2, substorms, *J. Geophys. Res., 84*, 4099, 1979*b*.

Kamide, Y., J. D. Craven, L. A. Frank, B.-H. Ahn, and S.-I. Akasofu, Modeling substorm current systems using conductivity distributions inferred from DE auroral images, *J. Geophys. Res., 91*, 11235, 1986.

Knight, S., Parallel electric fields, *Planet. Space Sci., 21*, 741, 1973.

Lyons, L. R., D. S. Evans, and R. Lundin, An observed relation between magnetic field aligned electric fields and downward electron energy fluxes in the vicinity of auroral forms, *J. Geophys. Res., 84*, 457, 1979.

Marklund, G. T, L. G. Blomberg, T. A. Potemra, J. S. Murphree, F. J. Rich, and K. Stasiewicz, A new method to derive "instantaneous" high-latitude potential distributions from satellite measurements including auroral imager data, *Geophys. Res. Lett., 14*, 439, 1987*a*.

Marklund, G. T., L. G. Blomberg, D. A. Hardy, and F. J. Rich, Instantaneous pictures of the high-latitude electrodynamics using Viking and DMSP/F7 observations, *ESA SP-270*, pp. 45, Proc. of 8th ESA/PAC Symposium, Sunne, Sweden, 17-23 May, 1987*b*.

Marklund, G. T., L. G. Blomberg, K. Stasiewicz, J. S. Murphree, R. Pottelette, L. J. Zanetti, T. A. Potemra, D. A. Hardy, and F. J. Rich, Snapshots of high-latitude electrodynamics using Viking and DMSP/F7 observations, *J. Geophys. Res., 93*, 14479, 1988.

Marklund, G. T., L. G. Blomberg, J. S. Murphree, R. D. Elphinstone, L. J. Zanetti, R. E. Erlandson, I. Sandahl, O. de la Beaujardière, H. Opgenoorth, and F. J. Rich, On the electrodynamical state of the auroral ionosphere during northward IMF: A transpolar arc case study, *J. Geophys. Res, 96*, 9567, 1991.

Marklund, G. T., and L. G. Blomberg, On the influence of localized electric fields and field-aligned currents associated with polar arcs on the global potential distribution, *J. Geophys. Res., in press*, 1991*a*.

Marklund, G. T., and L. G. Blomberg, Toward a better understanding of the global auroral electrodynamics through numerical modeling studies, *Proceedings of the Chapman conference on magnetospheric substorms, Hakone, 3-7 September 1990, in press*, 1991*b*.

Nisbet, J. S., M. J. Miller, and L. A. Carpenter, Currents and Electric Fields in the Ionosphere Due to Field-aligned Auroral Currents, *J. Geophys. Res., 83*, 2647, 1978.

Richmond, A. D., and Y. Kamide, Mapping electrodynamic features of the high-latitude ionosphere from localized observations: Technique, *J. Geophys. Res., 93*, 5741, 1988.

Rishbeth, H., and O. K. Garriot, Introduction to ionospheric physics, *Academic Press*, 1969.

Smith, G. D., Numerical solution of partial differential equations, *Oxford University Press*, 1965.

Tsyganenko, N. A., and A. V. Usmanov, Determination of the magnetospheric current system parameters and development of experimental geomagnetic field models based on data from IMP and HEOS satellites, *Planet. Space Sci., 30*, 985, 1982.

Tsyganenko, N. A., Global quantitative models of the geomagnetic field in the cislunar magnetosphere for different disturbance levels, *Planet. Space Sci., 35*, 1347, 1987.

Tsyganenko, N. A., A magnetospheric magnetic field model with a warped tail current sheet, *Planet. Space Sci., 37*, 5, 1989.

Vickrey, J. F., R. C. Livingston, N. B. Walker, T. A. Potemra, R. A. Heelis, M. C. Kelley, and F. J. Rich, On the current-voltage relationship of the magnetospheric generator at intermediate spatial scales, *Geophys. Res. Lett., 13*, 495, 1986.

Wallis, D. D., and E. E. Budzinski, Empirical models of height-integrated conductivities, *J. Geophys. Res., 86*, 125, 1981.

TRITA-EPP-91-03 ISSN 0348-7539

Department of Plasma Physics, Alfvén Laboratory,
Royal Institute of Technology, S-100 44 Stockholm, Sweden

A NUMERICAL MODEL OF IONOSPHERIC CONVECTION DERIVED FROM FIELD-ALIGNED CURRENTS AND THE CORRESPONDING CONDUCTIVITY

L. G. Blomberg and G. T. Marklund
August 1991, 29 pages incl. illustrations, in English

A numerical model for the calculation of ionospheric convection patterns from given distributions of field-aligned current and ionospheric conductivity is described. The model includes a coupling between the conductivity and the field-aligned current, so that the conductivity peaks in regions of upward current, as usually observed by measurements. The model is very flexible in that the input distributions, the field-aligned current and the conductivity, have been parametrized in a convenient way. From the primary model output, namely the ionospheric electrostatic potential (or convection) in the corotating frame, a number of other quantities can be computed. These include: the potential in the inertial frame (the transformation takes into account the non-alignment of the Earth's magnetic and geographic axes), the potential in the magnetospheric equatorial plane (projected using either a dipole magnetic field model or the Tsyganenko-Usmanov model, and the assumption of either vanishing parallel electric field or a proportionality between parallel potential and upward field-aligned current), the distribution of ionospheric (horizontal) current, and the Joule heating in the ionosphere. This model has been used together with a new snapshot technique to calculate the high-latitude potential distribution prevailing during a particular event by combining information from global auroral images and local measurements of fields and particles. The model potential variation along the satellite orbit was found to be in excellent agreement with that calculated from the measured electric field. The model has also been used to study some fundamental properties of the electrodynamics of the high-latitude ionosphere. The results of these different applications of the model have been published separately.

Key words: Ionospheric modelling, Ionospheric convection, Ionospheric electric fields, Ionospheric conductivities, Ionospheric currents, Field-aligned currents, Corotation, Ionosphere-Magnetosphere interaction, Auroral physics